Magnetism in the $R_5T_4Sn_{10}$ (R=Ce, Pr, and Nd; T=Rh and Ir) system

N. G. Patil and S. Ramakrishnan
Tata Institute of Fundamental Research, Bombay-400005, India
(Received 9 January 1997; revised manuscript received 22 April 1997)

We report the study of magnetism in a series of compounds of the type $R_5T_4Sn_{10}$ (R=Ce, Pr, and Nd; T=Rh and Ir) at low temperatures. Magnetization, resistivity, and heat-capacity studies show that the three compounds of the series $R_5Rh_4Sn_{10}$ undergo magnetic ordering below 10 K. The transition temperatures are 4.4, 5.5, and 7 K for Ce, Pr, and Nd compounds, respectively. There is a sharp anomaly in the heat-capacity and resistivity data of $Nd_5Rh_4Sn_{10}$ below 6.5 K which we attribute to a first-order magnetic transition. However, susceptibility, resistivity, and heat-capacity studies show that although $Ce_5Ir_4Sn_{10}$ orders antiferromagnetically below 4.2 K, $Pr_5Ir_4Sn_{10}$ remains paramagnetic down to 1.5 K. $La_5Ir_4Sn_{10}$ shows temperature-independent Pauli paramagnetism and does not exhibit superconductivity down to 1.5 K. The results are compared with that of $R_5Ir_4Si_{10}$ series. [S0163-1829(97)02230-3]

I. INTRODUCTION

Among the large number of ternary silicides which form in a variety of crystal structures, there exist a structure of the type $R_5T_4M_{10}$ (R=Dy to Lu, T=Co, Ir, and Rh, M=Si,Ge).[1] In this crystal structure ($Sc_5Co_4Si_{10}$, space group $P4/mbm$), there are neither transition metal clusters nor is there any direct transition-metal–transition-metal contact. This is in contrast to that of the RMo_6S_8 or RRh_4B_4 series which have been studied in great detail.[2–4] Some of the compounds belonging to the $R_5T_4M_{10}$ series undergo superconducting transition at low temperatures with charge-density wave (CDW)-type ordering at higher temperatures.[5,6] The compounds with magnetic rare-earth elements which order antiferromagnetically at low temperatures also show possible CDW or spin-density wave (SDW) transition at high temperatures ($T\sim$100 K).[7] Recently, we have established[8–11] a coexistence of superconductivity and magnetism in some pseudo-ternary alloys of this system. The light rare-earth elements (La, Ce, Pr, and Nd) do not form in this structure with Si or Ge. However, recent studies[12] have shown that these light rare-earth elements form compounds of the type $R_5T_4Sn_{10}$ (T=Rh,Ir) which have the same structure as that of $R_5T_4M_{10}$ system. We report the results of the susceptibility (1.5–300 K), resistivity (1.5–300 K), and heat-capacity (1.5–40 K) studies of these compounds. We also compare the nature of the magnetism exhibited by these compounds with those belonging to the $R_5Ir_4Si_{10}$ series.

II. EXPERIMENTAL DETAILS

Samples of $R_5T_4Sn_{10}$ (R=La, Ce, Pr, and Nd, T=Rh,Ir) were made by melting the individual constituents (taken in stoichiometric proportions) in an arc furnace under high-purity argon atmosphere. The purity of La, Ce, Pr, and Nd was 99.9% whereas the purity of Rh, Si were 99.95% and 99.999%, respectively. The alloy buttons were remelted six times to ensure proper mixing. The samples were annealed at 900 °C for a week. The x-ray powder diffraction pattern of the samples apart from $La_5Rh_4Sn_{10}$ and $Nd_5Ir_4Sn_{10}$ showed that these compounds form in the structure of the type $Sc_5Co_4Si_{10}$ ($P4/mbm$) without the presence of any parasitic impurity phases and the lattice constants a, c along with the density are given in Table I. Si is used as the internal standard for the powder diffraction measurements and the the lattice constants are determined using least square refinement. The errors in the estimated values of the lattice constants are given in brackets. The structure of the unit cell of the $R_5T_4Sn_{10}$ compound is illustrated in Fig. 1. However, the samples $La_5Rh_4Sn_{10}$ and $Nd_5Ir_4Sn_{10}$ contained multiphases (as inferred from x-ray analysis) and no measurements were made on those samples. Previous studies[12] also did not report the successful formation of the these two samples. The temperature dependence of the magnetic susceptibility (χ) was measured using a commercial superconducting quantum interference device (SQUID) magnetometer (Quantum Design MPMS 5, U.S.A.) in a field of 4 kOe in the temperature range from 2–300 K. A few isothermal magnetization runs were also made using the same magnetometer. The accuracy of the magnetization measurements is better than 1%. The ac susceptibility was measured using a home built susceptometer[13] from 1.5 to 20 K. The resistivity was measured using a four-probe dc technique with contacts made using silver paint on a cylindrical sample of 2 mm diameter and 10 mm length. The relative accuracy of the resistivity measurements is 100 ppm and the absolute accu-

TABLE I. Structural and normal state of properties of $R_5Rh_4Sn_{10}$ and $R_5Ir_4Sn_{10}$.

Sample	a(Å)	c(Å)	Density (gm/cc)
$Ce_5Rh_4Sn_{10}$	14.04±0.01	4.62±0.01	8.01
$Pr_5Rh_4Sn_{10}$	13.96±0.01	4.60±0.01	8.15
$Nd_5Rh_4Sn_{10}$	13.91±0.01	4.59±0.01	8.30
$La_5Ir_4Sn_{10}$	14.80±0.01	4.68±0.01	8.27
$Ce_5Ir_4Sn_{10}$	14.10±0.01	4.61±0.01	9.27
$Pr_5Ir_4Sn_{10}$	13.91±0.01	4.48±0.01	9.81

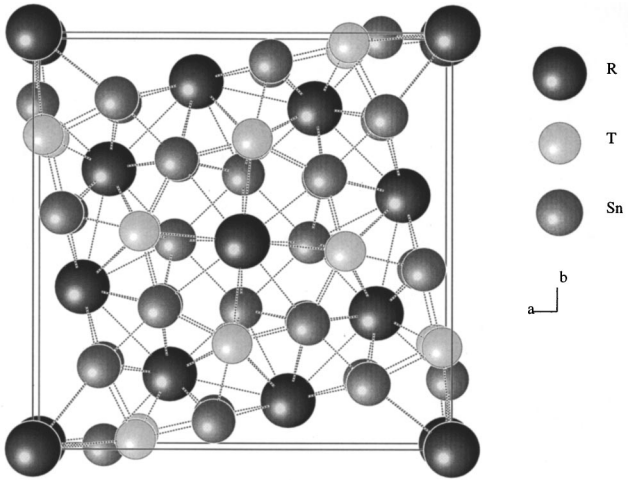

FIG. 1. Structure of the unit cell of the $R_5T_4Sn_{10}$ series.

racy of the resistivity measurements is only around 1% due to the error in the estimation of the geometrical factor of the samples. The temperature was measured using a calibrated Si diode (Lake Shore Inc., U.S.A.) sensor. The sample voltage was measured with a a nanovoltmeter (model 182, Keithley, U.S.A.) with a current of 25 mA using a 20 ppm stable (Hewlett Packard, U.S.A.) current source. All the data were collected using an IBM compatible PC/AT via IEEE-488 interface. The heat-capacity in zero field between 1.7 to 40 K was measured using an automated adiabatic heat pulse method. A calibrated germanium resistance thermometer (Lake Shore Inc, U.S.A.) was used as the temperature sensor in this range. The accuracy of the heat-capacity value is 1% over this temperature range.

III. RESULTS AND DISCUSSION

A. Magnetism in $Ce_5Rh_4Sn_{10}$

1. Magnetic susceptibility studies

The temperature dependence of the inverse dc magnetic susceptibility (χ_{dc}^{-1}) of the $Ce_5Rh_4Sn_{10}$ sample in a field of 4 kOe from 2 to 300 K is shown in Fig. 2. The inset shows susceptibility behavior of the same sample at low temperature. This inset clearly shows the antiferromagnetic transition below 4.4 K. It is possible that the Rudermann, Kittel, Kasuya, and Yosida (RKKY) interaction between the Ce^{3+} ions is responsible for the low-temperature ordering of Ce spins. However, at these low temperatures, there is also a possibility that the dipole-dipole interactions can also contribute to the observed antiferromagnetism. One requires estimation of the RKKY interaction using microscopic techniques such as NMR in this material in order to resolve this issue. The high-temperature susceptibility ($100<T<300$ K) is fitted to a modified Curie-Weiss expression which is given by

$$\chi=\chi_0+\frac{C}{(T-\theta_p)}, \tag{1}$$

where C is the Curie constant which can be written in terms of the effective moment as

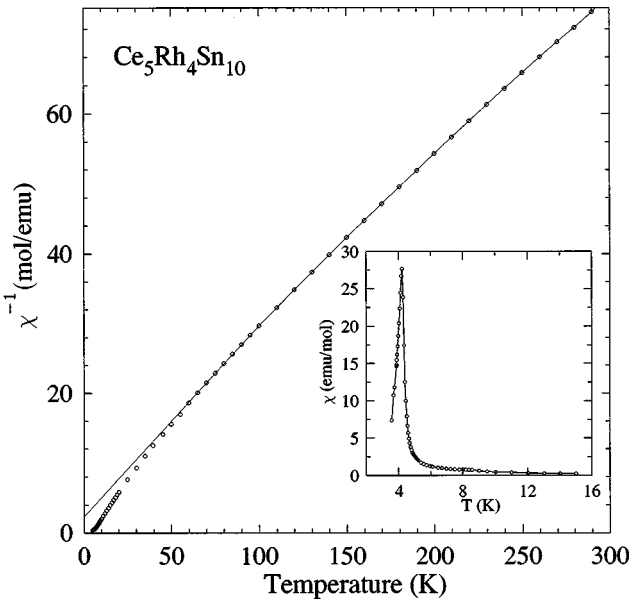

FIG. 2. Variation of the inverse susceptibility (χ^{-1}) of $Ce_5Rh_4Sn_{10}$ from 2 to 300 K. The inset shows the low-temperature χ data with the magnetic transition below 4.4 K.

$$C=\frac{\mu_{\text{eff}}^2 x}{8}, \tag{2}$$

where x is the concentration of Ce ions ($x=5$ for $Ce_5Rh_4Sn_{10}$). The values of χ_0, C, and θ_p are found to be 1.94×10^{-3} emu/mol, 3.43 emu K/mol, and -8.04 K, respectively. The main contributions to the temperature independent χ_0 are namely, the diamagnetic susceptibility which arises due to the presence of ion cores and the susceptibility of the conduction electrons. The estimated effective moment is found to be $2.34\mu_B$ which is smaller than the free ion moment of the Ce^{3+} ion ($2.54\mu_B$). The structure of $Ce_5Rh_4Sn_{10}$ has three sites for the Ce ion and it is possible that the valency of Ce is different from 3 in one or more sites which could account for the smaller effective moment compared to the free ion value. Similar observations have been made in $Ce_3Ru_4Ge_{13}$ (Ref. 14) (with two different sites for Ce), where the effective moment is only $1.35\mu_B$. Below 100 K, the χ data of $Ce_5Rh_4Sn_{10}$ show significant deviation from Curie-Weiss plot which could be due to the presence of crystal-field contributions.

2. Resistivity studies

The temperature dependence of the resistivity (ρ) $Ce_5Rh_4Sn_{10}$ is shown in Fig. 3. The inset shows the low-temperature ρ data on an expanded scale. The ρ data show a sharp fall at 4.4 K which is the antiferromagnetic transition temperature (T_n) of this sample. This is in accord with the T_n value obtained from χ data. In the paramagnetic state ($10<T<30$ K), the temperature dependence of ρ could be fitted to a power law which can be written as

$$\rho=\rho_0+aT^n. \tag{3}$$

The optimum value of n is found to be 3/2 and the values of ρ_0 and a are found to be 109 $\mu\Omega$ cm and 0.27 $\mu\Omega$ cm/K$^{3/2}$, respectively. This value of n suggests the presence

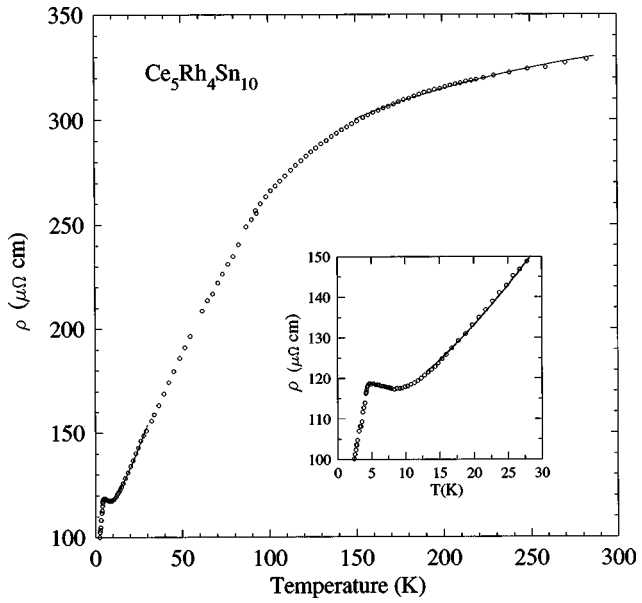

FIG. 3. Temperature dependence of resistivity (ρ) of $Ce_5Rh_4Sn_{10}$ from 2 to 300 K. The inset shows the low-temperature ρ data from 2 to 30 K. The solid lines are fits to the models (see text).

of ferromagnetic correlations or spin-glass-type excitations at these temperatures. However, magnetization measurements indicate only antiferromagnetic ordering below 4.4 K. At present, we do not understand the reason for this power-law (3/2) dependence. The high residual resistivity of 109 $\mu\Omega$ cm of the sample decreases sharply below 4 K due to magnetic ordering. Measurements below 2 K are required to study the influence of magnetic ordering on the resistivity of this sample. At high temperatures ($100<T<300$ K), the ρ data significantly deviates from the linear temperature dependence. Such a deviation from linear temperature dependence at high temperatures has been seen in many alloys where the saturation is attributed to the high value of ρ of these alloys at these temperatures. This deviation from linearity occurs because the mean-free path becomes short, of the order of few atomic spacings. When that happens, the scattering cross section will no longer be linear in the scattering perturbation. Since the dominant temperature-dependent scattering mechanism is the electron-phonon interaction here, the ρ will no longer be proportional to the mean square atomic displacement, which is proportional to T for a harmonic potential. Instead, the resistance will rise less rapidly than linearly in T and will show negative curvature ($d^2\rho/dT^2<0$). This behavior was also seen in previous studies on silicides and germanides.[15,16]

One of the models which describe the $\rho(T)$ of these compounds is known as the parallel resistor model.[17] In this model the expression of $\rho(T)$ is given by

$$\frac{1}{\rho(T)}=\frac{1}{\rho_1(T)}+\frac{1}{\rho_{\max}}, \tag{4}$$

where $\rho_{\max}$ is the saturation resistivity which is independent of temperature and $\rho_1(T)$ is the ideal temperature-dependent resistivity. Further, the ideal resistivity is given by the expression

TABLE II. Parameters obtained from the parallel resistor model fit in $R_5Rh_4Sn_{10}$.

Sample	$\rho_{\max}$	ρ_1	C	θ_D
$Ce_5Rh_4Sn_{10}$	447	155	866	167
$Pr_5Rh_4Sn_{10}$	467	49.3	639	196
$Nd_5Rh_4Sn_{10}$	609	44.8	600	135

$$\rho_1(T)=\rho_0+C_1\left(\frac{T}{\theta_D}\right)^3\int_0^{\theta_D/T}\frac{x^3dx}{[1-\exp(-x)][\exp(x)-1]}, \tag{5}$$

where $\rho(0)$ is the residual resistivity and the second term is due to phonon-assisted electron scattering similar to the *s-d* scattering in transition metal alloys. θ_D is the Debye temperature and C_1 is a numerical constant. Equation (4) can be derived if we assume that the electron mean-free path l is replaced by $l+a$ (a being an average interatomic spacing). Such an assumption is reasonable, since infinitely strong scattering can only reduce the electron mean-free path to a. Chakraborty and Allen[18] have made a detailed investigation of the effect of strong electron-phonon scattering within the framework of the Boltzmann transport equation. They find that the interband scattering opens up ''nonclassical channels'' which account for the parallel resistor model. The values of the various parameters obtained by fitting the data between 100 to 300 K to the parallel resistor model are given in Table II.

3. Heat-capacity studies

The temperature dependence of the heat capacity (C_p) from 2 to 35 K of $Ce_5Rh_4Sn_{10}$ is shown in Fig. 4. The inset shows the low temperature C_p vs T data. The jump in C_p at 4.4 K ($\Delta C=23$ J/mol K) clearly shows bulk magnetic ordering in this sample below this temperature. The temperature dependence of C_p is fitted to the expression,

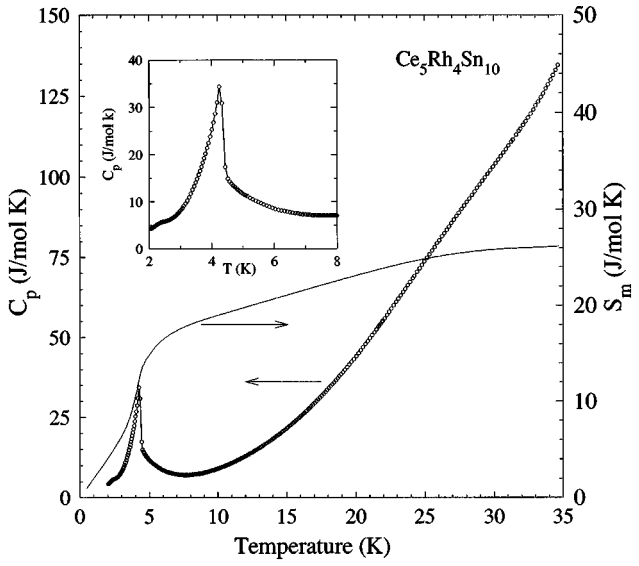

FIG. 4. Plot of C_p vs T of $Ce_5Rh_4Sn_{10}$ from 2 to 40 K. The inset shows the same plot from 2 to 10 K to illustrate the bulk magnetic ordering.

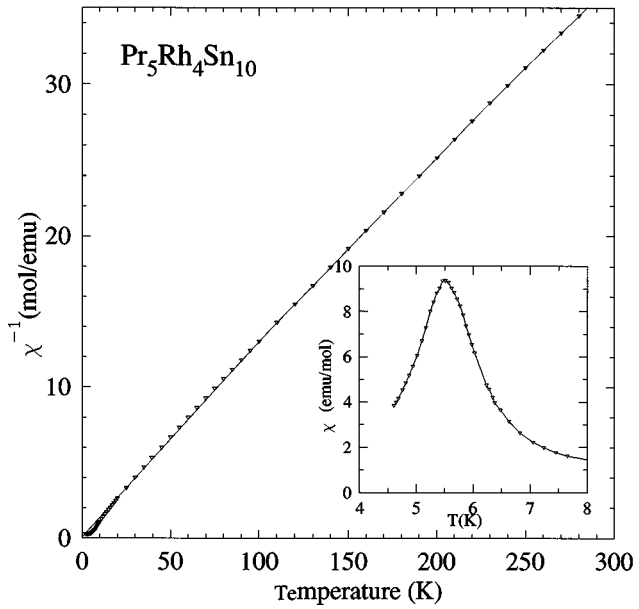

FIG. 5. Variation of inverse susceptibility (χ^{-1}) of $Pr_5Rh_4Sn_{10}$ from 2 to 300 K. The inset shows the low-temperature χ data with a slope change around 5.5 K.

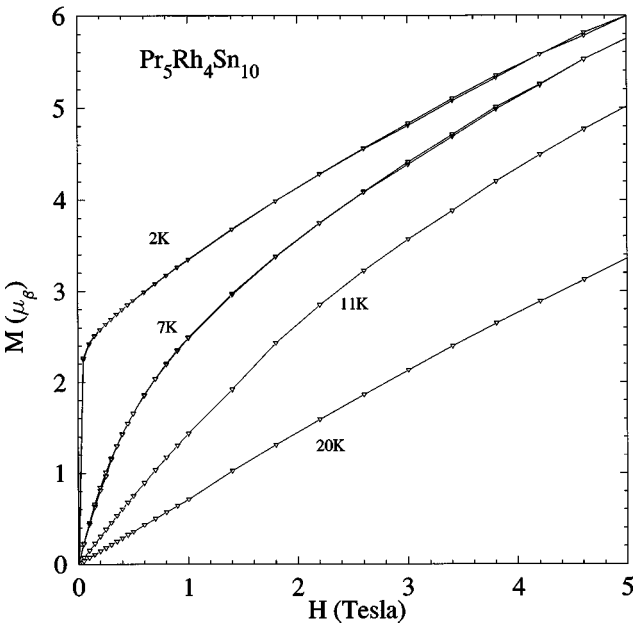

FIG. 6. Isothermal magnetization of $Pr_5Rh_4Sn_{10}$ at different temperatures. The observed curvature in the M vs H plot well above T_n suggests contributions from CEF effects. Metamagnetic transition occurs in this compound at very low fields.

$$C_p=\gamma T+\beta T^3, \tag{6}$$

where γ is due to the electronic contribution and β is due to the lattice contribution. The fit to the heat-capacity data using Eq. (6) in the temperature range from 10 to 20 K yielded 104 mJ/ Ce mol K^2 and 0.411 mJ/mol K^4 for γ and β, respectively. From the β value of 0.411 mJ/mol K^4, we estimate the θ_D to be 440 K using the relation

$$\theta_D=\left(\frac{12\pi^4 N r k_B}{5\beta}\right)^{1/3}, \tag{7}$$

where N is the Avogadro's number, r is the number of atoms per formula unit, and k_B is the Boltzmann's constant. The value of 104 mJ/Ce mol K^2 for γ suggests that $Ce_5Rh_4Sn_{10}$ is a moderate heavy fermion antiferromagnet. However, C_p measurements down to 0.3 K are needed to confirm this view. Entropy above 30 K found to be 5.2 J/Ce mol K which is less than the expected value of $R\ln(2J+1)$, and shows that crystal field contributions are present. The total entropy below T_n is found to be 2 J/mol K, which is significantly less than the value of $R\ln 2$ (entropy for the magnetic doublet) and this shows the existence of antiferromagnetic correlations above T_n.

B. Magnetism in $Pr_5Rh_4Sn_{10}$

1. Magnetic susceptibility studies

The temperature dependence of the inverse dc magnetic susceptibility (χ_{dc}^{-1}) of the $Pr_5Rh_4Sn_{10}$ sample in a field of 4 kOe from 2 to 300 K is shown in Fig. 5. The inset shows the susceptibility behavior of the same sample at low temperatures. This inset clearly indicates the antiferromagnetic ordering of Pr spins below 5.5 K. As in the case of $Ce_5Rh_4Sn_{10}$, we expect the RKKY interaction to be mainly responsible for the observed antiferromagnetic ordering in this alloy. The high-temperature susceptibility ($100K<T<300$ K) is fitted to a modified Curie-Weiss expression which is given by Eq. (1) with $\chi_0=0$. The values of θ_p and μ_{eff} are found to be -0.72 K and $3.47\mu_B$, respectively. The estimated effective moment of 3.47 μ_B is slightly lower than the free ion moment of the Pr^{3+} ion ($3.58\mu_B$). Below 100 K, the χ data show deviation from Curie-Weiss plot which could be due to the presence of crystal-field contributions. Figure 6 shows the isothermal magnetization data of $Pr_5Rh_4Sn_{10}$ at various temperatures from 2 to 20 K. At higher temperatures ($T>T_n$), one observes nonlinear behavior in the magnetization which can be attributed to crystalline electric field (CEF) effects. However, at low temperatures ($T<T_n$), one observes a large jump in the magnetization at low fields with very little hysteresis in the forward and reverse direction of the field sweep. This could be due to a spin-flop transition. However, more magnetization studies (preferably in single-crystal samples) are necessary to justify this speculation.

2. Resistivity studies

The temperature dependence of the resistivity (ρ) of $Pr_5Rh_4Sn_{10}$ is shown in Fig. 7. The inset shows the low-temperature ρ data on an expanded scale. The ρ data show a change of slope at 5.5 K which is the antiferromagnetic ordering temperature (T_n) of this sample. This is same as the T_n value obtained from χ data. In the paramagnetic region ($10<T<30$ K), the temperature dependence of ρ could be fitted to a linear T dependence in contrast to the $T^{3/2}$ dependence observed in $Ce_5Rh_4Sn_{10}$. The residual resistivity ratio (RRR) of the $Pr_5Rh_4Sn_{10}$ compound is rather high (RRR$\approx$60) and the linear temperature dependence of ρ is quite puzzling. However, below 5.5 K, the resistivity shows a power-law dependence in T (T^n, where $n\geqslant 2$). At high temperatures, the ρ behavior is similar to that observed in

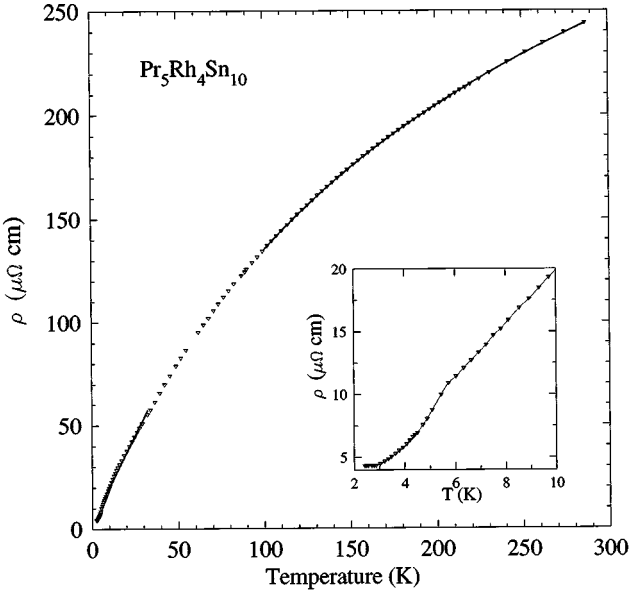

FIG. 7. Temperature dependence of resistivity (ρ) of $Pr_5Rh_4Sn_{10}$ from 2 to 300 K. The inset shows the low-temperature ρ data from 2 to 30 K. A small kink in ρ near 5.5 K in the inset indicates antiferromagnetic ordering in this compound. The solid lines are fit to the models (see text).

$Ce_5Rh_4Sn_{10}$ and the data could be fitted to the parallel resistor model. The values of the fitted parameters are given in Table II.

C. Heat-capacity studies on $Pr_5Rh_4Sn_{10}$

The temperature dependence of C_p from 2 to 35 K of $Pr_5Rh_4Sn_{10}$ is shown in Fig. 8. The inset shows the low-temperature C_p data. The large jump at 5.5 K ($\Delta C = 6.1$ J/mol K) clearly shows bulk magnetic ordering in this sample. This temperature is slightly lower than the T_n value

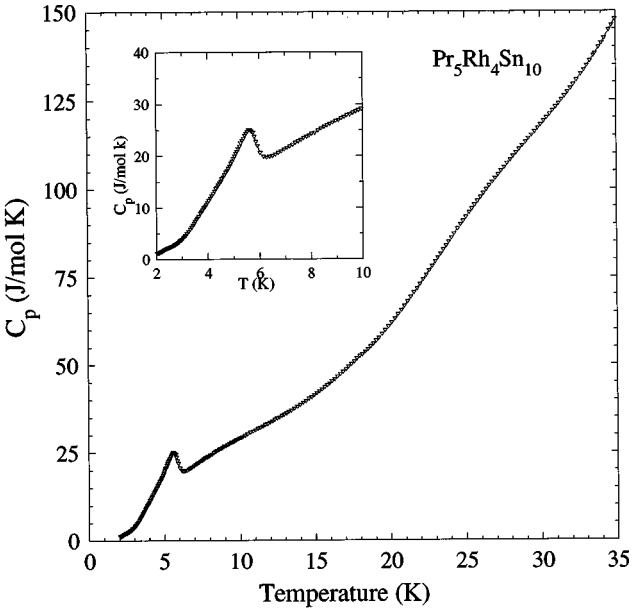

FIG. 8. Plot of C_p vs T of $Pr_5Rh_4Sn_{10}$ from 2 to 40 K. The inset shows the same plot from 2 to 10 K. A large jump of 6.1 J/mol K signifies bulk magnetic ordering of Pr^{3+} spins.

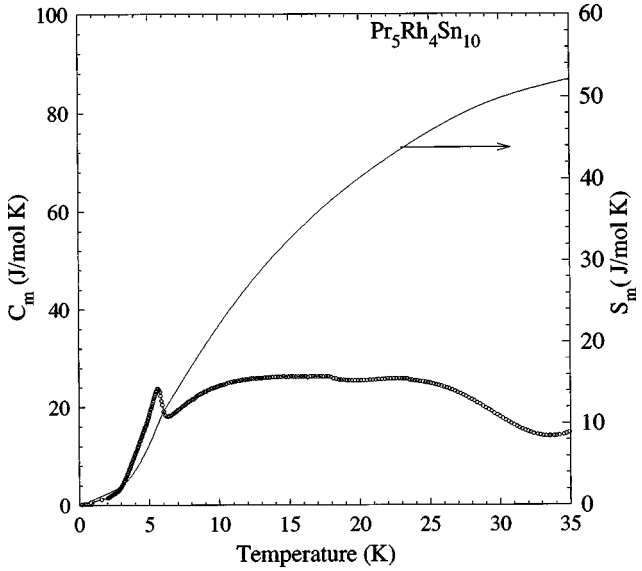

FIG. 9. Magnetic contribution to the heat capacity and entropy for $Pr_5Rh_4Sn_{10}$ from 2 to 35 K.

observed from the χ, as well as the ρ measurements. From these observations, we conclude that this sample undergoes antiferromagnetic ordering below 5.5 K. The magnetic contribution to the heat capacity (which is obtained after subtracting the measured C_p data from that of $La_5Ir_4Sn_{10}$) is shown in Fig. 9. The calculated entropy is also shown in the same figure. Entropy above 30 K found to be 10.4 J/Pr mol K which is less than expected value of $R\ln(2J+1)$; this signifies a contribution from crystal-field effects in this sample. The total entropy below T_n is found to be 2.5 J/mol K, which is significantly less than the value of $R\ln 2$ (entropy for the magnetic doublet) and this shows the existence of antiferromagnetic correlations above T_n. Preliminary calculations suggest that the next excited state is also a doublet and its separation from this doublet ground state is approximately 42 K. Exact calculation of the crystal-field contribution to the heat-capacity, susceptibility, and resistivity requires a detailed model which is in progress and will be published elsewhere. From the high-temperature heat-capacity data, we estimate the Debye temperature for this sample to 400 K, which disagrees with the result obtained from the resistivity analysis.

D. Magnetism in $Nd_5Rh_4Sn_{10}$

1. Magnetic susceptibility studies

The temperature dependence of the inverse dc magnetic susceptibility (χ_{dc}^{-1}) of the $Nd_5Rh_4Sn_{10}$ sample in a field of 4 kOe from 2 to 300 K is shown in Fig. 10. The low-temperature χ behavior is shown in the inset. One finds that the Nd moments order anitferromagnetically below 7 K in this alloy. As in the case of other two alloys, we expect the RKKY interaction to be mainly responsible for the antiferromagnetism below 7 K in this alloy. The high-temperature susceptibility ($100 < T < 300$ K) is fitted to a modified Curie-Weiss expression which is given by Eq. (1) and the values of θ_p and μ_{eff} are found to be -3.8 K and $3.92\mu_B$, respectively. The estimated effective moment of $3.92\mu_B$ is higher

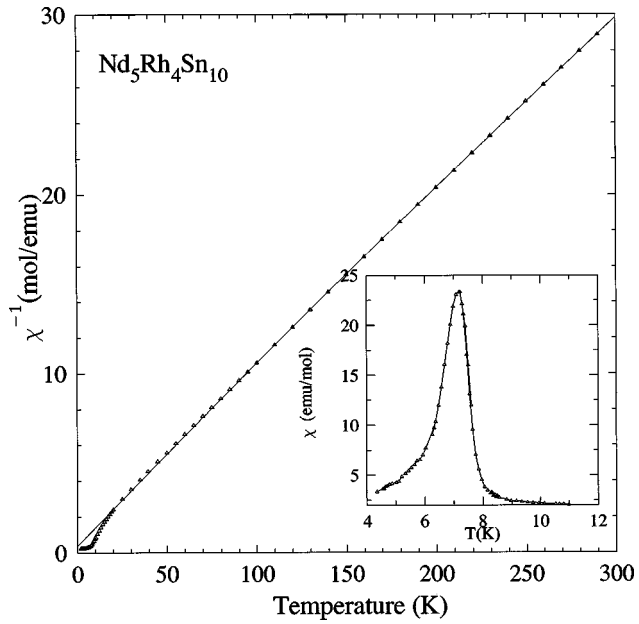

FIG. 10. Variation of inverse susceptibility (χ^{-1}) of $Nd_5Rh_4Sn_{10}$ from 2 to 300 K. The inset shows the low-temperature χ data with a slope change around 7.0 K.

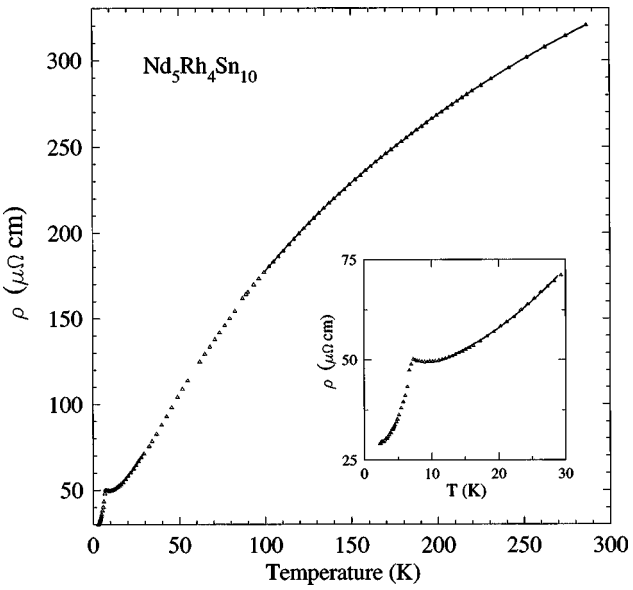

FIG. 12. Temperature dependence of resistivity (ρ) of $Nd_5Rh_4Sn_{10}$ from 2 to 300 K. The inset shows the low-temperature ρ data from 2 to 30 K. A small kink in ρ near 7.0 K in the inset indicates antiferromagnetic ordering in this compound. The solid lines are fit to the models (see text).

than the free ion moment of the Nd^{3+} ion ($3.62\mu_B$). This suggests the contribution from conduction electrons of the Rh band to the effective moment. Below 100 K, the χ data show a deviation from the Curie-Weiss plot which could be due to the presence of crystal-field excitations. The isothermal magnetization data at 5 and 20 K are shown in Fig. 11. At 20 K, we observe usual paramagnetic behavior of the Nd^{3+} ions with a linear M vs H in contrast to the nonlinear behavior observed in $Pr_5Rh_4Sn_{10}$. However, we observe a magnetic transition below 5 K at low fields similar to the one

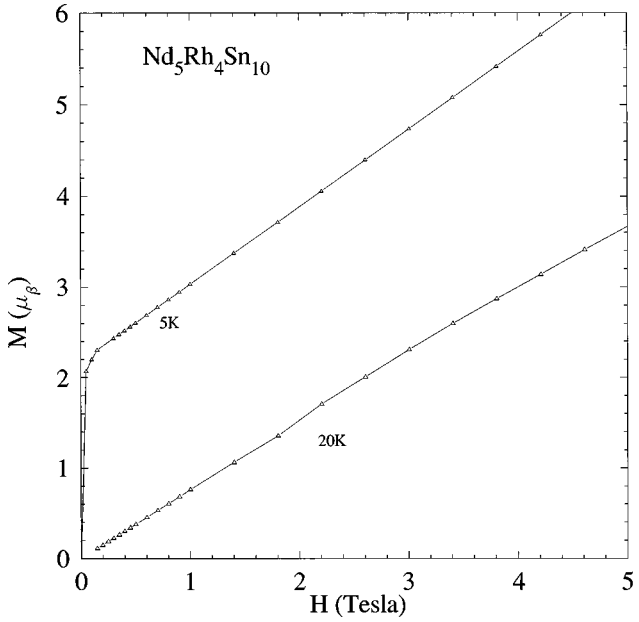

FIG. 11. Isothermal magnetization of $Nd_5Rh_4Sn_{10}$ at different temperatures. The usual linear M vs H plot well above T_n suggests paramagnetism and it is different from that of $Pr_5Rh_4Sn_{10}$. Magnetic transition also occurs in this compound at very low fields.

observed in the Pr sample. Ferromagnetic ordering is ruled out because there was no measurable hysteresis in the forward and reverse cycles.

2. Resistivity studies

The temperature dependence of the resistivity (ρ) of $Nd_5Rh_4Sn_{10}$ is shown in Fig. 12. The inset shows the low-temperature ρ data on an expanded scale. The ρ data show a change of slope at 7.0 K which is the antiferromagnetic ordering temperature (T_n) of this sample. This is in accord with the T_n value obtained from χ data. In the temperature range ($10<T<30$ K), the temperature dependence of ρ could be fitted to the T^2 dependence which suggests that the spin fluctuations play a dominant role in scattering the conduction electrons. The low-temperature resistivity fit yields a value of 46 $\mu\Omega$ cm and 30 $\mu\Omega$ cm/K^2 for ρ_0 and a, respectively. There is a sudden jump in the resistivity data below 6.5 K which is not present in the χ measurements. We attribute this behavior in ρ to a first-order antiferromagnetic magnetic transition involving incommensurate to commensurate transition at 6.5 K. We confirm the first-order transition by the observation of a small hysteresis in the ρ data in the cooling and warming cycle as shown in Fig. 13. Further, the heat-capacity measurements (discussed in the next section) also support this conclusion. At high temperatures, the ρ behavior is similar to that observed in $Ce_5Rh_4Sn_{10}$ and $Pr_5Rh_4Sn_{10}$. The values of the fitted parameters to the parallel resistor model are given in Table II.

E. Heat-capacity studies on $Nd_5Rh_4Sn_{10}$

The temperature dependence of C_p from 2 to 35 K of $Nd_5Rh_4Sn_{10}$ is shown in Fig. 14. The inset shows the low-temperature C_p data. The C_p data show two large jumps at 7 and 6.5 K, respectively. The first jump at 7 K ($\Delta C=28$

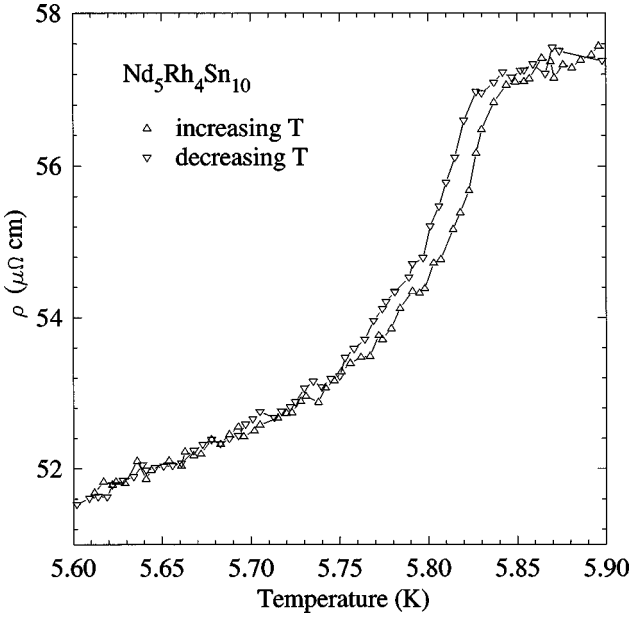

FIG. 13. Hysteresis in the temperature dependence of resistivity (ρ) of $Nd_5Rh_4Sn_{10}$ from below T_n. This hysteresis although small ($\approx$50 mK) suggests first order magnetic transition.

J/mol K) clearly shows bulk magnetic ordering Nd^{3+} ions in this sample. But even larger and a sharper jump ($\Delta C = 250$ J/mol K) at 6.5 K shows the evidence of first-order antiferromagnetic ordering in the absence of structural transition (inferred from powder x-ray data at low temperatures) at this temperature. Similar observations are recently reported in CePdAl system by Donni *et al.*[19] However, detailed neutron-scattering measurements are required to understand this transition. These measurements are in progress and will be reported elsewhere. The magnetic contribution to the heat capacity (which is obtained after subtracting the measured C_p data from that of $La_5Ir_4Sn_{10}$) is also shown in Fig. 15.

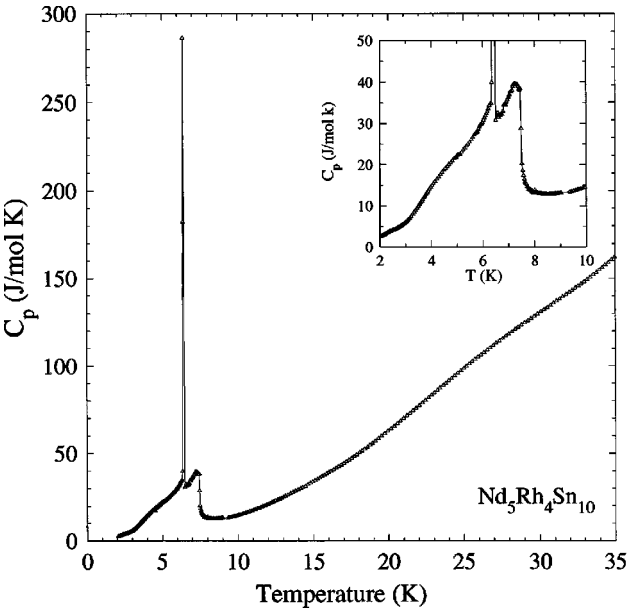

FIG. 14. Plot of C_p vs T of $Nd_5Rh_4Sn_{10}$ from 2 to 40 K. The inset shows the same plot from 2 to 10 K. A large jump of 28 J/mol K signifies bulk magnetic ordering of Nd^{3+} spins.

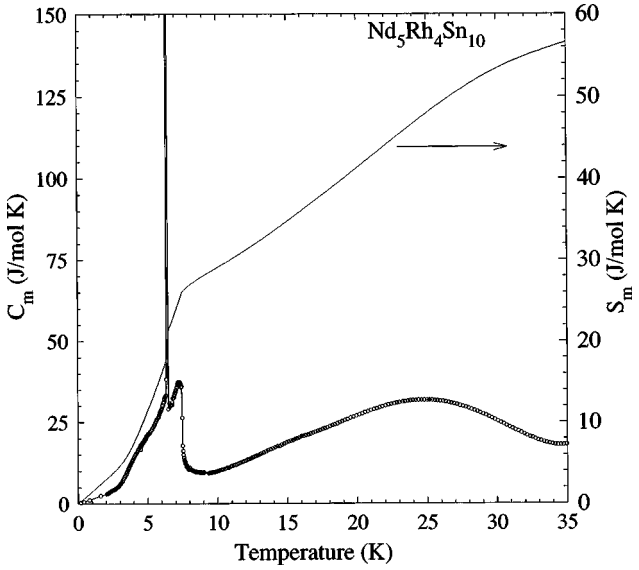

FIG. 15. Magnetic contribution to the heat capacity and entropy for $Nd_5Rh_4Sn_{10}$ from 2 to 35 K.

The calculated entropy is also shown in the same figure. Entropy above 30 K found to be 11.2 J/Nd mol K which is less than expected value of $R\ln(2J+1)$, this signifies contribution from CEF in this sample. The total entropy below T_n is found to be 4.4 J/mol K, which is almost equal to the value of $R\ln 2$ and this shows that the ground state is a doublet. Preliminary calculations support this view and the next excited state is also a doublet and its separation from this doublet ground state is approximately 50 K. Exact calculation of the crystal-field contribution to the heat-capacity, susceptibility, and resistivity requires a detailed model which is in progress and will be published elsewhere. From the high-temperature heat-capacity data, we estimate the Debye temperature for this sample to be 300 K, which is much larger than the result obtained from the resistivity analysis which is quite puzzling. Moreover, the γ value is of the order of 200 mJ/Nd mol K^2 which is very large and the reason for this large value is not understood. Heat-capacity data below 2 K are needed to understand this behavior.

F. Magnetism in $Ce_5Ir_4Sn_{10}$

1. Magnetic susceptibility studies

The temperature dependence of the inverse dc magnetic susceptibility (χ_{dc}^{-1}) of the $Ce_5Ir_4Sn_{10}$ sample in a field of 4 kOe from 2 to 300 K is shown in Fig. 16. The inset shows susceptibility behavior of the same sample at low temperature. This inset clearly shows the antiferromagnetic transition below 4.2 K. As in the case with Rh compounds, we beleive that the major contribution towards the magnetic ordering arises from the indirect Rudermann, Kittel, Kasuya, and Yosida (RKKY) interaction between the Ce^{3+} ions. It is interesting to note that there is only small decrease in the antiferromagnetic ordering temperature in $Ce_5Ir_4Sn_{10}$ compared to that of $Ce_5Rh_4Sn_{10}$ ($T_n = 4.4$ K). The high-temperature susceptibility ($100 < T < 300$ K) is fitted to a modified Curie-Weiss expression which is given by Eq. (1). The values of χ_0, C, and θ_p are found to be 1.58×10^{-3}

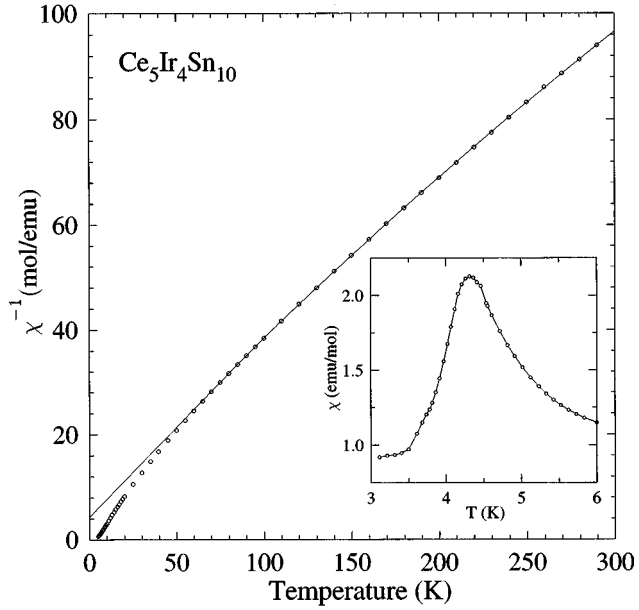

FIG. 16. Variation of inverse susceptibility (χ^{-1}) of $Ce_5Ir_4Sn_{10}$ from 2 to 300 K. The inset show the low-temperature χ data with the magnetic transition below 4.2 K.

emu/mol, 2.7326 emu K/mol, and -11.88 K, respectively. The main contributions to the temperature independent χ_0 are, namely, the diamagnetic susceptibility which arises due to the presence of ion cores and the susceptibility of the conduction electrons. The estimated effective moment is found to be $2.09\mu_B$ which is smaller than the free ion moment of the Ce^{3+} ion ($2.54\mu_B$). As in the case of $Ce_5Rh_4Sn_{10}$, the structure of $Ce_5Ir_4Sn_{10}$ has three sites for the Ce ion and it is possible that the valency of Ce is different from 3 in one or more sites which could account for the smaller effective moment compared to the free ion value.

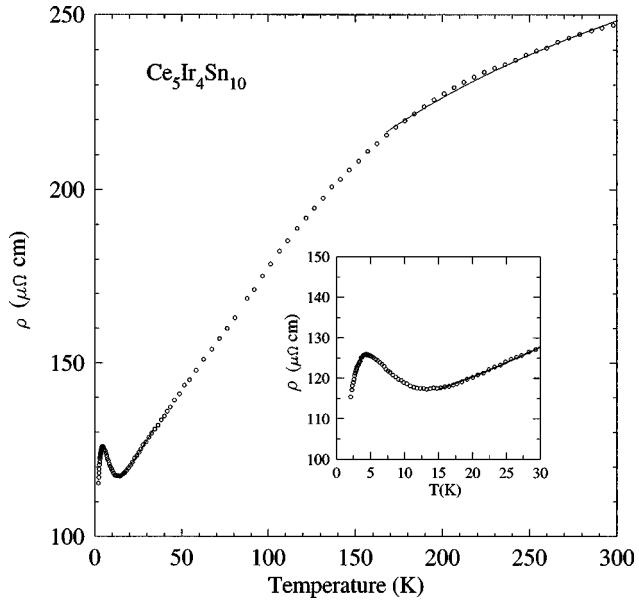

FIG. 17. Temperature dependence of resistivity (ρ) of $Ce_5Ir_4Sn_{10}$ from 2 to 300 K. The insets show the low-temperature ρ data from 2 to 30 K. The solid lines are fits to the models (see text).

TABLE III. Parameters obtained from the low-temperature resistivity fit in $R_5Rh_4Sn_{10}$ and $R_5Ir_4Sn_{10}$.

Sample	$\rho_0\mu\Omega$	a	n
$Ce_5Rh_4Sn_{10}$	109	0.27	1.5
$Pr_5Rh_4Sn_{10}$	5	4.4	1
$Nd_5Rh_4Sn_{10}$	46	0.034	2
$La_5Ir_4Sn_{10}$	16.6	0.00034	3
$Ce_5Ir_4Sn_{10}$	116	0.0987	1.5
$Pr_5Ir_4Sn_{10}$	78.4	2.2	1

Below 100 K, the χ data show a deviation from the Curie-Weiss plot which could be due to the presence of crystal-field contributions.

2. Resistivity studies

The temperature dependence of the resistivity (ρ) $Ce_5Ir_4Sn_{10}$ is shown in Fig. 17. The inset shows the low-temperature ρ data on an expanded scale. The ρ data show a minimum around 14 K followed by a sharp rise up to 4.2 K and then a rapid fall at 4.2 K which is the antiferromagnetic transition temperature (T_n) of this sample. This is in agreement with the T_n value obtained from χ data. The minima at 14 K and the subsequent rise in ρ could be associated with the formation of superzone gaps which arise when the lattice periodicity is incommensurate with the periodicity magnetic ordering. Similar observations have been made in $Dy_5Ir_4Si_{10}$.[20] In the paramagnetic state ($10<T<30$ K), the temperature dependence of ρ could be fitted to a power law using Eq. (3). The values of the parameters for the best fit are given in Table III. The high residual resistivity of 125 $\mu\Omega$ cm of the sample decreases sharply below 4.2 K due to magnetic ordering. Measurements below 2 K are required to study the influence of magnetic ordering on the resistivity of this sample. At high temperatures ($100<T<300$ K), the ρ data significantly deviates from the linear temperature dependence similar to that of other members in this series. The values of the various parameters obtained by fitting the data between 100 to 300 K to the parallel resistor model are given in Table IV.

3. Heat-capacity studies

The temperature dependence of the heat capacity (C_p) from 2 to 35 K of $Ce_5Ir_4Sn_{10}$ is shown in Fig. 18. The inset shows the low-temperature C_p vs data. The jump in C_p at 4.2 K ($\Delta C=18$ J/mol K) clearly shows bulk magnetic ordering in this sample below this temperature. The fit to the heat-capacity data using Eq. (6) in the temperature range from 10 to 20 K yielded 108 mJ/Ce mol K^2 and 0.40 mJ/mol K^4 for

TABLE IV. Parameters obtained from the parallel resistor model fit in $R_5Ir_4Sn_{10}$.

Sample	$\rho_{max}\mu\Omega$	$\rho_1\mu\Omega$	C $\mu\Omega$	θ_DK
$La_5Ir_4Sn_{10}$	778	35	615	312
$Ce_5Ir_4Sn_{10}$	337	223	1106	225
$Pr_5Ir_4Sn_{10}$	323	248	786	135

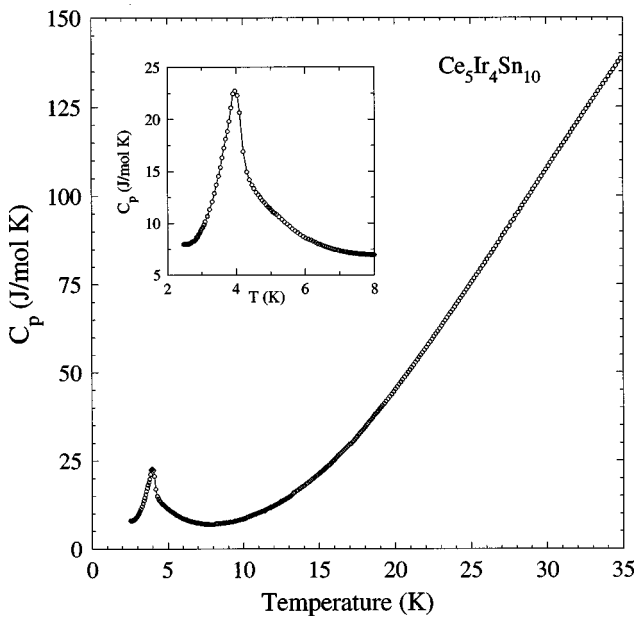

FIG. 18. Plot of C_p vs T of $Ce_5Ir_4Sn_{10}$ from 2 to 35 K. The inset shows the same plot from 2 to 8 K to illustrate the bulk magnetic ordering.

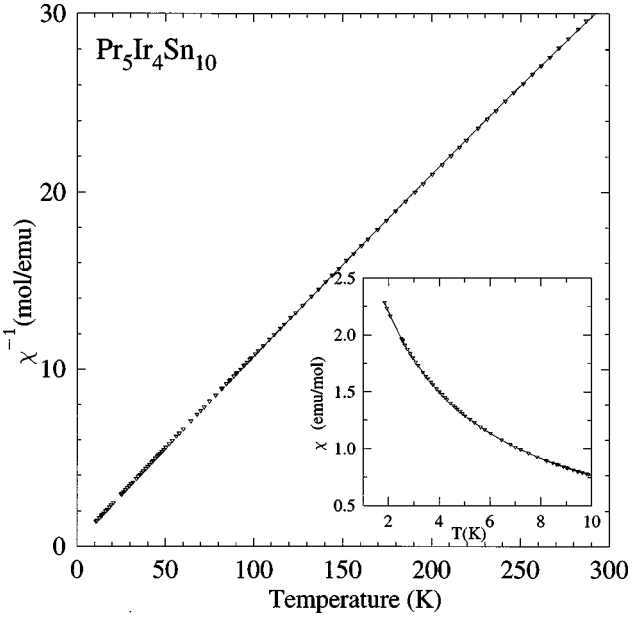

FIG. 19. The temperature dependence of the inverse susceptibility (χ^{-1}) of $Pr_5Ir_4Sn_{10}$ from 2 to 300 K. The inset shows the low-temperature χ data.

γ and β, respectively. From the β value of 0.40 mJ/mol K^4, we estimate the θ_D to be 443 K using the relation (7). The value of 108 mJ/Ce mol K^2 for γ suggests that $Ce_5Ir_4Sn_{10}$ is a moderate heavy fermion antiferromagnet. However, C_p measurements down to 0.3 K are needed to confirm this view.

G. Magnetism in $Pr_5Ir_4Sn_{10}$

1. Magnetic susceptibility studies

The temperature dependence of the inverse dc magnetic susceptibility (χ_{dc}^{-1}) of the $Pr_5Ir_4Sn_{10}$ sample in a field of 4 kOe from 2 to 300 K is shown in Fig. 19. The inset shows the susceptibility behavior of the same sample at low temperatures. This inset shows paramagnetic behavior of Pr spins down to 1.5 K. It is possible that we have a nonmagnetic singlet ground state for Pr in this compound. However, we need to confirm this using neutron-scattering studies at low temperatures. The high-temperature susceptibility ($100<T<300$ K) is fitted to a modified Curie-Weiss expression which is given by Eq. (1) with $\chi_0=0.0$ emu/mol. The values of θ_p and μ_{eff} are found to be -2.19 K and $3.86\mu_B$, respectively. The estimated effective moment of $3.86\mu_B$ is slightly higher than the free ion moment of Pr^{3+} ion ($3.58\mu_B$). This probably indicates a contribution from Ir band to the effective moment. Below 100 K, the χ data show very small deviation from Curie-Weiss plot which could be due to the presence of crystal-field contributions. This is in contrast to that of $Ce_5Rh_4Sn_{10}$ where we see a large deviation in χ due to crystal-field effects.

2. Resistivity studies

The temperature dependence of the resistivity (ρ) of $Pr_5Ir_4Sn_{10}$ is shown in Fig. 20. The inset shows the low-temperature ρ data on an expanded scale. The ρ data show a change of slope at 3 K which has no correspondence with χ data. In the temperature range ($10<T<30$ K), the temperature dependence of ρ could be fitted to a linear T dependence in contrast to the $T^{1.5}$ dependence observed in $Ce_5Ir_4Sn_{10}$. The fact that the residual resistivity ratio (RRR) of the sample is greater than 6 suggests a good quality sample and the linear dependence of ρ is quite puzzling. The values of the parameters used in the low-temperature resistivity fit [Eq. (3)] are given in Table III. At high temperatures, the ρ behavior is similar to that observed in

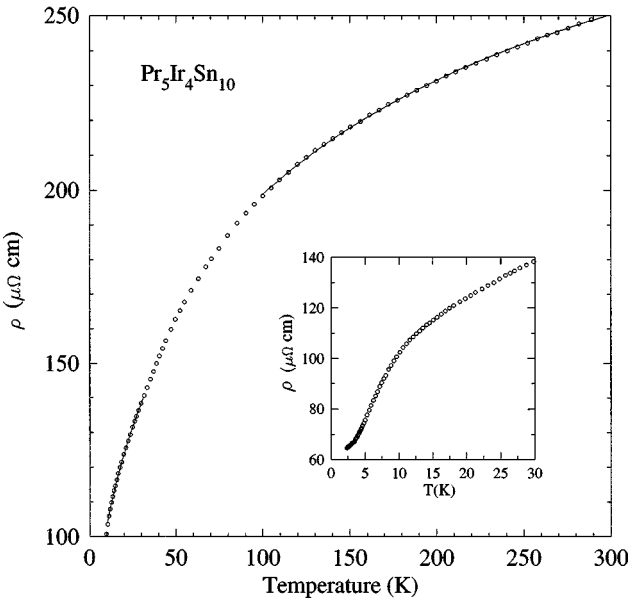

FIG. 20. Temperature dependence of resistivity (ρ) of $Pr_5Ir_4Sn_{10}$ from 2 to 300 K. The inset shows the low-temperature ρ data from 2 to 30 K. A slope change in ρ near 3 K in the inset has no correspondence with the χ data. The solid lines are fit to the models (see text).

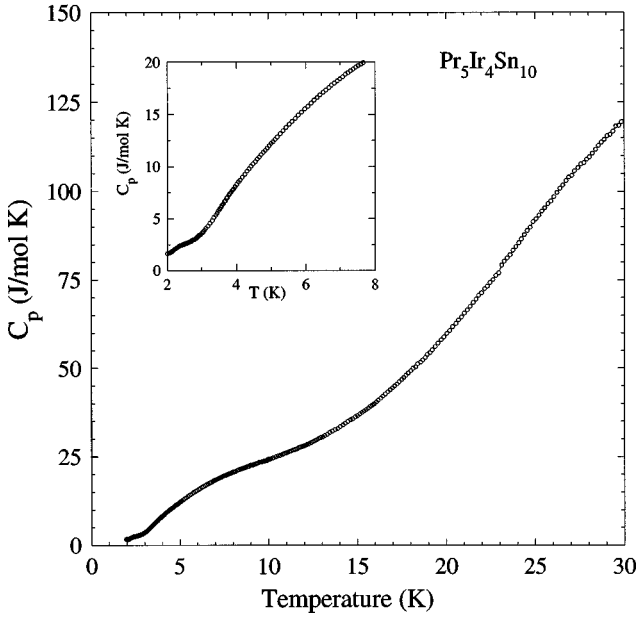

FIG. 21. Plot of C_p vs T of $Pr_5Ir_4Sn_{10}$ from 2 to 40 K. The inset shows the same plot from 2 to 10 K. A large value of 375 mJ/Pr mol K^2 suggests heavy-fermion behavior in this system.

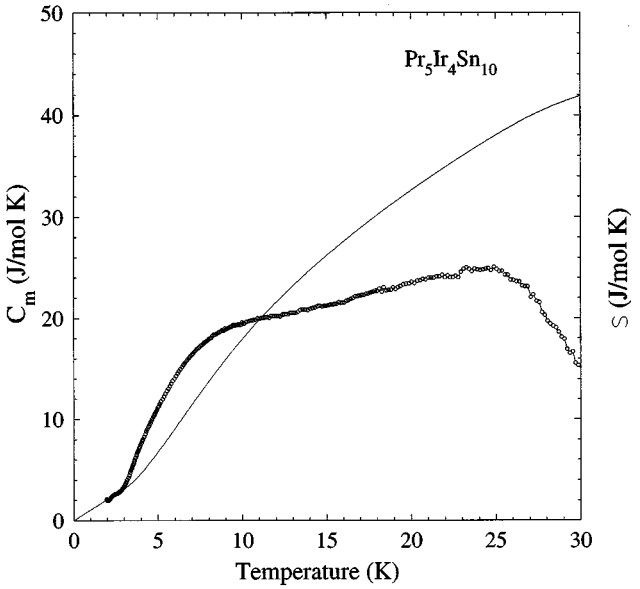

FIG. 22. Magnetic contribution to the heat capacity and entropy for $Pr_5Ir_4Sn_{10}$ from 2 to 30 K.

$Ce_5Ir_4Sn_{10}$ and the data could be fitted to the parallel resistor model. The values of the fitted parameters are given in Table IV.

H. Heat-capacity studies on $Pr_5Ir_4Sn_{10}$

The temperature dependence of C_p from 2 to 35 K of $Pr_5Ir_4Sn_{10}$ is shown in Fig. 21. The inset shows the low-temperature C_p data. The absence of a peak in C_p clearly shows nonbulk magnetic ordering in this sample down to 2 K. This is in agreement with the χ and ρ measurements. However, there are changes of slope in C_p below 10 and 3 K which are not understood at this moment. The magnetic contribution to the heat capacity (obtained after subtracting the measured C_p data from that of $La_5Ir_4Sn_{10}$) is shown in Fig. 22. The calculated entropy is also shown in the same figure. The increase in the entropy at high temperatures ($T>20$ K) signifies contribution from crystal-field effects in this sample. Exact calculation of the crystal-field contribution to the heat capacity, susceptibility, and resistivity requires a detailed model which is in progress and will be published elsewhere. From the high-temperature heat-capacity data, we estimate the Debye temperature for this sample to be 225 K, which is higher than the result obtained from the resistivity analysis. The large value of 354 mJ/Pr mol K^2 for the Sommerfeld coefficient γ suggests that $Pr_5Ir_4Sn_{10}$ is a nonmagnetic heavy fermion compound. However, heat-capacity studies well below 2 K are essential to resolve this issue. Similar results for Pr compounds have been reported recently.[21,22]

I. Physical properties of $La_5Ir_4Sn_{10}$

1. Magnetic susceptibility studies

The temperature dependence of the inverse dc magnetic susceptibility (χ_{dc}^{-1}) of the $La_5Ir_4Sn_{10}$ sample in a field of 4 kOe from 4 to 300 K is shown in Fig. 23. The inset shows the susceptibility behavior of the same sample at low temperatures. The normal state χ_{dc} of this sample has a temperature independent value of 3.8×10^{-4} emu/mol down to 10 K. Below 10 K, there is a small increase (3%) in χ_{dc} which we attribute to the presence of paramagnetic impurities in this sample. The temperature independent χ_{dc} has contributions from the core diamagnetism, Landau diamagnetism, and Pauli paramagnetism. This can be expressed as

$$\chi_{dc}-\chi_{core}=S(\chi_{Landau}+\chi_{Pauli}), \tag{8}$$

where S is the Stoner enhancement factor. This can be further simplified as,

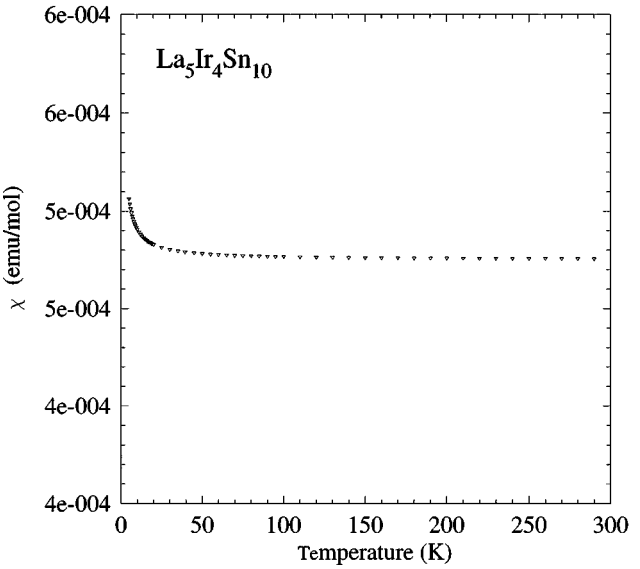

FIG. 23. The temperature dependence of inverse susceptibility (χ) of $La_5Ir_4Sn_{10}$ with temperature from 2 to 300 K.

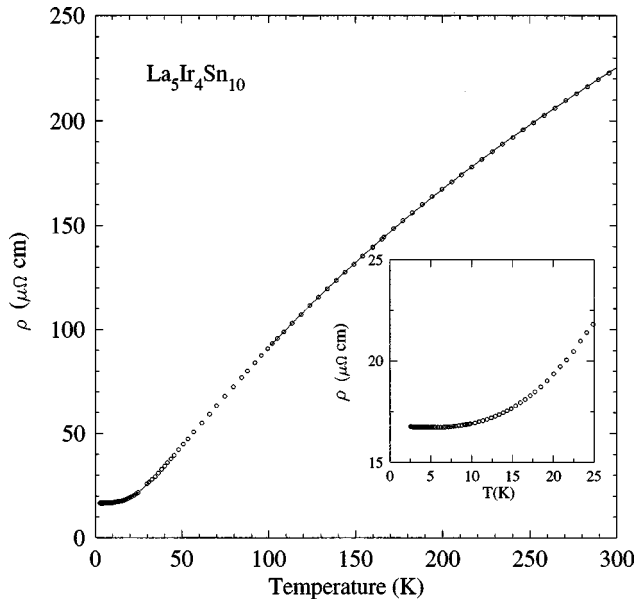

FIG. 24. Temperature dependence of resistivity (ρ) of $La_5Ir_4Sn_{10}$ from 2 to 300 K. The inset shows the low-temperature ρ data from 2 to 30 K. The solid lines are fits to the models (see text).

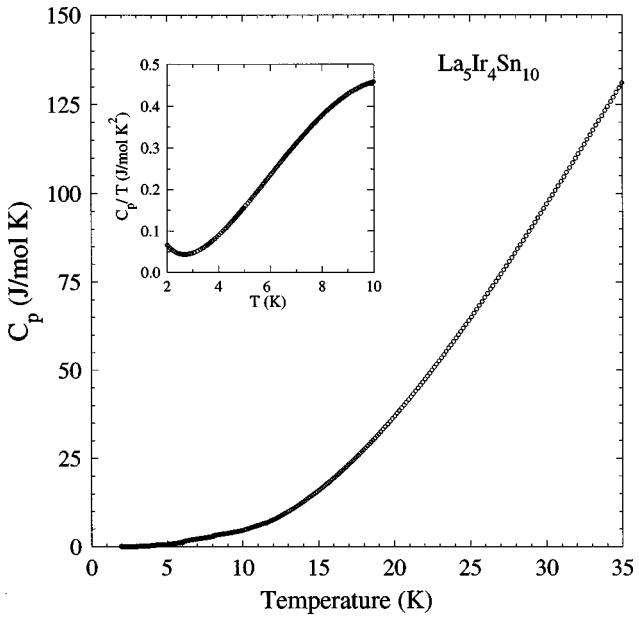

FIG. 25. Plot of C_p vs T of $La_5Ir_4Sn_{10}$ from 2 to 40 K. The inset shows the same plot from 2 to 10 K.

$$\chi_{\rm dc}-\chi_{\rm core}=S\chi_{\rm Pauli}\left[1-\frac{1}{3}\left(\frac{m}{m_b}\right)\right],$$

where $\chi_{\rm Pauli}=nN_A\mu_B^2N(E_F)$ is the Pauli susceptibility, μ_B is the Bohr magneton, m is the free electron mass, and m_b is the band mass. Assuming the valence of La as 3, Ir as 3, and Sn as 4, we estimate the core diamagnetism to be -2×10^{-4} emu/mol. We have also calculated the value of the Pauli susceptibility as 2.1×10^{-4} emu/mol and this yields a value of 2.75 for the Stoner factor of $La_5Ir_4Sn_{10}$.

2. Resistivity studies

The temperature dependence of the resistivity (ρ) of $La_5Ir_4Sn_{10}$ is shown in Fig. 24. The inset shows the low-temperature ρ data on an expanded scale. In the low-temperature region ($5<T<25$ K), the temperature dependence of ρ could be fitted to a power law which is given by Eq. (1). The values of the parameters for this fit are given in Table III. The optimum value of n is found to be 3. This value of n agrees with the Wilson's s-d scattering model which predicts a T^3 dependence of $\rho(T)$ for $T<\theta_D/10$.

At high temperatures ($100<T<300$ K), the ρ data significantly deviates from the linear temperature dependence similar to those of the $Ce_5Ir_4Sn_{10}$ and $Pr_5Ir_4Sn_{10}$ samples. The data could be fitted to the parallel resistor model and the values of the parameters are given in Table IV.

3. Heat-capacity studies

The temperature dependence of the heat capacity (C_p) from 2 to 35 K of $La_5Ir_4Sn_{10}$ is shown in Fig. 25. The inset shows the low-temperature C_p/T vs T data. The fit to the heat capacity data using Eq. (6) in the temperature range from 5 to 8 K yielded 29 mJ/mol K^2 and 0.4 mJ/mol K^4 for γ and β, respectively. From the β value of 0.4 mJ/mol K^4, we estimate the θ_D to be 339 K using the relation given by Eq. (7).

IV. CONCLUSION

We have observed magnetic ordering below 10 K in the $R_5Rh_4Sn_{10}$ (R=Ce, Pr, and Nd) system. These ordering temperatures are comparable to those of the $R_5Ir_4Si_{10}$ system. In the structure of the $R_5Rh_4Sn_{10}$ series, there are no transition-metal clusters and this structure can be described by the stacking of two types of building blocks, namely, trigonal prisms SnR_6 and distorted tetragonal antiprisms $Rh(Ir)Sn_4R_4$. The unit cell has 38 atoms. All Rh(Ir)-Sn and Sn-Sn distances are short (2–2.5 Å) which indicate strong covalent interactions. As we mentioned earlier, the rare-earth atoms have three different sites to occupy and the minimum distance between any two rare-earth atoms is greater than 5 Å. Moreover, the bond distance between rare earth R in any one of the three sites with the Rh atom is greater than 3 Å. These distances are large enough so that the exchange interaction between the magnetic rare-earth atom and the conduction electrons is weak. This could account for the low magnetic ordering temperature observed in these compounds. However, the compounds belonging to the $R_5Rh_4Sn_{10}$ series undergo a spin-flop transition at very low fields compared to the $R_5Ir_4Si_{10}$ ones. It is not clear whether the increase in the conduction electron density (which is larger in the Sn series compared to the Si series) is the cause for this unusual magnetic ordering. We observe a first-order magnetic transition in $Nd_5Rh_4Sn_{10}$ as evidenced by the hysteresis in the resistivity and a sharp peak in the heat-capacity data. Neutron-scattering experiments will help us to know whether one has incommensurate to commensurate magnetic transition (similar to the one observed in CePdAl by Donni *et al.*[19]) in this compound. However, $Pr_5Rh_4Sn_{10}$ undergoes antiferromagnetic ordering at 5.5 K whereas, $Pr_5Ir_4Sn_{10}$ exhibits para-

magnetism down to 1.5 K. The increase in the unit-cell volume (which is larger in Ir compared to the Rh series) which leads to a decrease in the strength of the RKKY interaction could be responsible for the absence of magnetic ordering in $Pr_5Ir_4Sn_{10}$. The heavy-fermion behavior in this compound is interesting and requires further study for confirmation. Microscopic investigations such as neutron scattering are clearly required to understand the nature of magnetism and crystal-field states in the $R_5Rh_4Sn_{10}$ (R=Ce and Pr) system. The absence of a CDW transition in the $R_5T_4Sn_{10}$ series could be due to their large unit-cell volume compared to that of the $R_5Ir_4Si_{10}$ series.

[1] H. F. Braun, in *Ternary Superconductors*, edited by G. K. Shenoy, B. D. Dunlap, and F. Y. Fradin (North-Holland, Amsterdam, 1980), p. 225.

[2] See the papers in *Superconductivity in Ternary Compounds*, edited by M. B. Maple and O. Fisher (Springer-Verlag, Berlin, 1984), Vol. II.

[3] O. Pena and M. Sergent, Prog. Solid State Chem. **19**, 165 (1989).

[4] O. Fisher, in *Ferromagnetic Materials*, edited by K. H. J. Buschow and E. P. Wohlfarth (Elsevier, Holland, 1990), Chap. 6.

[5] H. D. Yang, P. Klavins, and R. N. Shelton, Phys. Rev. B **43**, 7681 (1991).

[6] B. Becker *et al.* (unpublished).

[7] K. Ghosh, S. Ramakrishnan, and Girish Chandra, Phys. Rev. B **48**, 4152 (1993).

[8] S. Ramakrishnan, K. Ghosh, and Girish Chandra, Phys. Rev. B **46**, 2958 (1992).

[9] S. Ramakrishnan, K. Ghosh, Arvind D. Chinchure, Kristian Jonason, V. R. Marathe, and Girish Chandra, Phys. Rev. B **51**, 8398 (1995).

[10] K. Ghosh, S. Ramakrishnan, Arvind D. Chinchure, K. Jonason, V. R. Marathe, Girish Chandra, and S. S. Shah, Phys. Rev. B **51**, 11 656 (1995).

[11] S. Ramakrishnan and K. Ghosh, Physica B **223&224**, 154 (1996).

[12] G. Venturini, B. Malaman, and B. Roques, Mater. Res. Bull. **24**, 1135 (1989).

[13] S. Ramakrishnan, S. Sundaram, R. S. Pandit, and Girish Chandra, J. Phys. E **18**, 650 (1985).

[14] K. Ghosh, S. Ramakrishnan, S. K. Dhar, S. K. Malik, Girish Chandra, V. K. Pecharsky, K. A. Gschneidner, Jr., Z. Hu, and W. B. Yelon, Phys. Rev. B **52**, 7267 (1995).

[15] S. Ramakrishnan, K. Ghosh, and Girish Chandra, Phys. Rev. B **45**, 10 769 (1992).

[16] K. Ghosh, S. Ramakrishnan, and Girish Chandra, Phys. Rev. B **48**, 10 440 (1993).

[17] H. Wiesmann, M. Gurvitch, H. Lutz, A. K. Ghosh, B. Schwarz, M. Strongin, P. B. Allen, and J. W. Halley, Phys. Rev. Lett. **38**, 782 (1977).

[18] B. Chakraborty and P. B. Allen, Phys. Rev. Lett. **42**, 736 (1979).

[19] A. Donni, H. Kitazawa, P. Fisher, J. Tang, M. Kohgi, Y. Endoh, and Y. Morii, J. Phys. Condens. Matter **7**, 1663 (1995).

[20] S. Ramakrishnan, K. Ghosh, and Girish Chandra, Phys. Rev. B **45**, 10 769 (1992).

[21] S. Ramakrishnan, K. Ghosh, S. K. Dhar, S. K. Malik, and Girish Chandra, J. Magn. Magn. Mater. **152**, 375 (1996).

[22] A. Yatskar, W. P. Beyermann, R. Movshovich, and P. C. Canfield, Phys. Rev. Lett. **77**, 3637 (1996).